Quasicrystals as superposed waves. Stability and entropy

Sofiane Benakli, Daniel Mercier, Jean-Claude Serge Lévy

Research Signpost
37/661 (2), Fort P.O.
Trivandrum-695 023
Kerala, India

Nanostructures and their Magnetic Properties, 2009: 37-71 ISBN: 978-81-308-0371-5
Editor: Jean-Claude Serge Lévy

3. Quasicrystals as superposed waves: Stability and entropy

Sofiane Benakli, Daniel Mercier and Jean-Claude Serge Lévy
Lab. Quantum Materials and Phenomena, CNRS UMR 7162 10 rue Alice Domon et Léonie Duquet, 75013 Paris, France

Abstract. 2D and 3D quasicrystalline structures are derived from an energy minimization method as a sum of density waves. The quasicrystalline stability against the occurrence of defects is controlled by the density difference between retained sites and possible defects. The relative stabilities of octagonal, decagonal, dodecagonal and icosahedral quasicrystals are compared. Sevenfold and elevenfold symmetry are shown to be quite instable. In the case of dodecagonal quasicrystals, the comparison between different solutions reveals their different densities and defects so their respective entropies are compared as well as their elastic and acoustic properties. Different quasicrystalline structures with a given symmetry can be produced by this method which reveals and classifies low energy defects.

1. Introduction

Since the first materials obtained by rapid quenching by Duwez and co-workers [1], quite numerous rather stable metallic glasses [2] have been obtained. A lot of these materials showed a local icosahedral symmetry [3] as

Correspondence/Reprint request: Dr. Jean-Claude Serge Lévy, Laboratoire Matériaux et Phénomènes Quantiques, UMR 7162 CNRS, Université Paris 7 Denis Diderot, 10 rue Alice Domon et Léonie Duquet 75013 Paris, France. E-mail: jean-claude.levy@univ-paris-diderot.fr

observed during the seventies. So it was interesting to search for solutions with optimal internal energy and icosahedral symmetry for a seed. This was done for materials interacting according to pair potentials [4]. It evidenced solutions with infinitely extended icosahedral symmetry [5]. A few years later, the diffraction patterns of such structures which are close to metallic glasses were observed with numerous delta-lines and infinitely extended icosahedral symmetry [6]. Some authors [7] proposed to call these structures with the already used name "quasicrystal" [8] which had different meanings before and was soon definitely retained for such structures. Another physical approach of what are now called quasicrystals was linked with the idea of intermediate structures between solids and liquids, with the famous example of liquid crystals [9] and the more recent notion of "hexatic" materials [10] where the transition from local properties to global properties is focused. Now thousands of materials [11] with properties which are associated with the class of quasicrystalline materials, i.e. materials with sharp diffraction peaks and without crystalline symmetry, have been observed. Moreover similar instantaneous quasicrystalline materials which result from wave superposition have also been observed [12].

This rapid emergence of a previously forbidden state as well as the possibility of different ways for accessing the structure of such materials suggests the existence of some "prehistoric" tracks of quasicrystals. Quasicrystalline symmetry was forbidden by standard crystallography since it is not compatible with translation. So even this introductory part requires some classification before defining its precise scope!

1.1. Prehistory of "multidisciplinary" quasicrystals

As just suggested we give a list of possible approaches of quasicrystals.

1.1.1. A physical approach of quasicrystals comes from the very local analysis of metallic glasses [2, 3] where **icosahedra** were observed at an atomic scale.

1.1.2. In chemistry, the observation of icosahedra was already a classical topic for **boron** structures [13], but such icosahedra were assumed to be merged in an overall crystalline structure [14].

1.1.3. In mathematics, 2D **selfsimilar** constructions using set of tiles with noncrystalline symmetry already led to quite regular noncrystalline structures. This was the case with Penrose rhombi [15], Robinson triangles [16], Ammam and Beenker squares and rhombi [17]. And such structures lead to diffraction patterns made of numerous delta-like lines [18].

1.1.4. Another physical approach of the quasicrystalline structures came from the structural and crystallographic analysis of another class of materials:

commensurate and **incommensurate** materials [19] where two or more periods are competing together. Usually in such materials there is a well defined overall period, but some other periods appear, with a commensurate or not ratio with the main period. So these other periods act as perturbations of the main structure. Quite obviously with complex materials such as biological ones, such competing periods happen often [20]. This remark reduces to a remark on **number theory** about such ratios [21]. So there are quite numerous interwoven origins of quasicrystals.

1.1.5. The more recent observation of **wave superposition** with quasicrystalline symmetry [22] can be also considered as another prehistoric source of quasicrystals since their history is just beginning.

1.1.6. In Islamic art, crystallographic objects were produced a long time before crystallography was introduced [23], and finite tiling with quasicrystalline properties was also produced a long time ago in many places, with quite different means [24]. It must be added that art and architecture took advantage of such explorations, with the examples of Vauban, Escher or Vasarely for instance.

1.2. Brief overview of theoretical quasicrystalline constructions

As already said these quasicrystalline features are strongly interwoven. So we will try to introduce different theoretical ways of building such structures and their interconnections.

1.2.1. A first approach of quasicrystalline structures is obviously the geometric approach. For instance, in a regular pentagon, diagonal cuts define two kinds of triangles, namely “darts” and “kites” and their self similar reductions. And these self similar cuts can be continued up to infinity [15, 16]. A special feature is this self-similarity ratio: the **golden number** $\tau = \frac{\sqrt{5}+1}{2}$. This means that there are both symmetry group properties and number theory properties which are involved in this point. So this defines an **algebraic** approach of quasicrystals [25].

1.2.2. A second approach of quasicrystalline structures is the energetic approach [4]. It comes from a **variational minimization** of the energy as due to pair interactions and it leads to the equation for Fourier transforms of the atomic density and pair potentials: $n_q \, V_q = 0$. This equation is solved with as a result an atomic density which is a symmetric sum of delta functions in reciprocal space, i.e. a sum of waves. This defines quasicrystals when locating atoms at density summits. Rather obviously the diffraction patterns of these structures are also made of delta functions with the same symmetry.

Of course this approach of quasicrystalline structures is related to other energetic approaches such as **steepest descent relaxation** [4, 26], **Monte-Carlo relaxation** under convenient interactions [27], or **ab initio** calculations derived from density functional theory for atomic clusters [28, 29].

1.2.3. A third approach comes from the commensurate-incommensurate structures where the energy minimization leads to introduce a fictitious N dimensional space in which there is a crystalline optimal structure with N dimensions. Finally the real space structure is deduced from this extra-space by a **cut and project** method [30]. There is a strong similarity between this method and the energy minimization which is the basis of this method.

1.2.4. A fourth "**crystallographic**" method comes from the experimental evidence of delta-functions peaks in the Fourier transform of the atomic density [31]. Of course this method is finally quite similar to the energy minimization method already introduced since there the atomic density results from the sum of delta functions in Fourier transforms, exactly as in an inverse problem.

1.2.5. A fifth "**acoustical**" method comes from the superposition of waves as experimentally observed [22]. Of course this method is quite analogous with the energetic method where the atomic density results from a sum of waves.

As a conclusion of this brief overview, the energetic method is the most synthetic "physical" method. The link between this method and mathematical data such as self similarity and number theory properties associated with such a self similar ratio must be underlined. This defines a first goal of this paper, with the transition from 1D and 2D density functions towards discrete set of points.

1.3. Stability and entropy of quasicrystals

A structure is stable in front of other possible structures if the internal or free energy of this structure is lower than the internal or free energy of its competing structures. The practical way for obtaining these competing structures consists in a thermodynamic production of defects which can aggregate within the initial structure and produce a competing structure. So the analysis of **defects** is crucial for stability study. Moreover the evaluation of entropy is also linked with **defect** numbering within a class of admitted energy variation. So the analysis of defects is also crucial for entropy estimation.

A first view about defects in quasicrystals comes from the old physical meaning of quasicrystals [8], an intermediate state between crystal and amorphous solid. In a crystal defects are quantified as interstitials and vacant

sites, with just a few interstitial sites per unit cell, while in amorphous solids or glasses, there is a continuum of intermediate configurations which can even vary slowly with time. So, in quasicrystals numerous defects are expected to occur. In crystals, clusters of defects occur often as it happens with colour centres [32], so clusters of defects are also expected in quasicrystals.

In the selfsimilar definition of quasicrystals [15-17], there are obviously several ways of defining cuts for the initial tiles, so even if matching rules between the individual parts [33] can restrict the number of variants of a quasicrystalline structure, there are necessarily several variants for each quasicrystal and so a resulting entropy. In the cut and project method [30], the cutting space can be shifted, and this defines quite numerous variants for a quasicrystal and so entropy appears too.

Another idea for classifying quasicrystals and crystals with a given symmetry comes from the fact that quite different crystalline structures such as face centred cubic (fcc) system, body centred cubic (bcc) system and simple cubic (sc) system share the same symmetry group, in the classical case of octahedral symmetry. So, this example leads to assume that different quasicrystals could also share the same quasicrystalline symmetry group [34]. Since quasicrystals define a superspace, these different quasicrystals could be defined in the same way as fcc, bcc and sc are in real 3D space, i.e. by introducing different convenient seed structures in the quasicrystalline superspace. Since these superspaces have more than three dimensions, there are more than three different seeds to consider for quasicrystals.

These remarks define two other goals to the present paper, first classifying defects in the energetic method and second building different quasicrystalline structures with the same symmetry at least for a given symmetry and comparing these structures.

1.4. Nanoquasicrystals

The main observed properties of quasicrystals are hardness with brittle fracture [35], and low conductivity in front of that of crystalline materials [36]. The property of hardness comes from the very long range ordering which is very strict in quasicrystals. And the high resistivity of quasicrystals is due to multiple electronic scattering due to the numerous directions with partial order in quasicrystals. With the general interest in nanomaterials, it sounds useful to look at nanoquasicrystals. Nanoquasicrystals can be as hard as quasicrystals, without the disadvantage of brittle fracture and their transport properties can be different from that of bulk quasicrystals since scattering is considerably reduced. Thus quasicrystals of nanometric size are of interest when immersed

in a convenient material for several properties. Magnetic properties of quasicrystals emphasize the existence of different non equivalent sites [37], with a stabilization of magnetic topological defects such as vortices. This could lead to applications for high density magnetic read and write process.

In section 2 the details of the energetic method are reported for pure materials and alloys. In section 3 the density function in 1D is considered with evidence for defects. In section 4, the density function in 2D is considered and the so-deduced quasicrystals are shown and analysed. The quasicrystal diffraction patterns are briefly reported in section 5 while section 6 deals with defects and entropy of quasicrystals in conclusion.

2. The energetic method

2.1. The principle: Interaction energy

This method is based upon the consideration of pair interactions as in the Bragg-Williams model [38] since pair interaction is the basic interaction, at least for metals without covalent binding. So two atoms located at sites $\vec{x}$ and $\vec{y}$ have an interaction energy $V(\vec{x},\vec{y})=V(\vec{x}-\vec{y})$. Assuming an atomic density $n(\vec{x})$ at site $\vec{x}$, this gives the total interaction energy due to the pair potential $V(\vec{x}-\vec{y})$:

$$E=\frac{1}{2}\int n(\vec{x})n(\vec{y})V(\vec{x}-\vec{y})d\vec{x}d\vec{y} \tag{1}$$

The discrete version of this approach on lattice with a small parameter was treated early and leads to similar results at the expense of heavy calculations [4]. In the more general case where there are different species, two atoms of species *i* and *j* respectively located respectively at sites $\vec{x}$ and $\vec{y}$ have an interaction energy $V_{ij}(\vec{x},\vec{y})=V_{ij}(\vec{x}-\vec{y})$. Assuming for species *i* an atomic density $n_i(\vec{x})$ at site $\vec{x}$, the total interaction energy is due to the pair potentials $V_{ij}(\vec{x}-\vec{y})$

$$E=\frac{1}{2}\sum_{ij}\int n_i(\vec{x})n_j(\vec{y})V_{ij}(\vec{x}-\vec{y})d\vec{x}d\vec{y} \tag{2}$$

The research for an optimal structure is made from a variational treatment of the energy. And the linearity of interactions shows that the solution is easily found after a Fourier transform, i.e. in reciprocal space [4],

since interaction between two occupied sites is easily derived as a convolution property. So, the Fourier transforms read:

$$n_i(\vec{x}) = C\int n_i(\vec{p})\exp(i\vec{p}*\vec{x})d\vec{p}$$
$$V_{ij}(\vec{x}) = C'\int V_{ij}(\vec{p})\exp(i\vec{p}*\vec{x})d\vec{p} \quad (3)$$

And the interaction energy is now :

$$E = \frac{1}{2}\sum_{ij}\int n_i{}^*(\vec{p})n_j(\vec{p})V_{ij}(\vec{p})d\vec{p} \quad (4)$$

This equation is quite simpler than equation (2) since it contains a single integration over the common wavevector $\vec{p}$.

2.2. The characteristic equation in reciprocal space

First with only one atomic species, a pure case, infinitesimal wavy variations of the atomic density are introduced, in order to check the optimal energy:

$$\delta n(\vec{p}) = C\delta(\vec{p}-\vec{p}_0)$$

Here the delta-function implies that the variation just occurs at the wavevector $\vec{p}_0$, i.e. a sinelike variation in real space. And such a variation does not change the global density. The variational equation reads, when assuming a real atomic density:

$$n(\vec{p})V(\vec{p}) = 0 \quad (5)$$

This equation means that the Fourier transform of the atomic density is non zero only for the nodes of the Fourier transform of the pair potential. A detailed treatment assuming that the wavevector $\vec{p}_0$ is a simple node, i.e. that $V'(\vec{p}_0) \neq 0$ shows that the Fourier transform of the atomic density is a sum of delta functions located at the nodes of the Fourier transform of the pair potential:

$$n(\vec{p}) = \sum C_k \delta(\vec{p}-\vec{p}_k), \text{ with } V(\vec{p}_k = 0) \quad (6)$$

Coming back to real space, this means that the atomic density results from a sum of sine waves:

$$n(\vec{x}) = \sum_k C_k \exp(i\vec{p}_k * \vec{x}) \tag{7}$$

Equation (6) has strong consequences for the structure factor [40], it means that the structure factor of this material is a sum of delta functions:

$$S(\vec{q}) = \langle n(\vec{q}) n(-\vec{q}) \rangle = \sum C'_k \, \delta(\vec{p} - \vec{p}_k) + \sum C''_{k,k'} \, \delta(\vec{p} - \vec{p}_k - \vec{p}_{k'}) \tag{8}$$

This already means that the diffraction pattern is also a sum of delta functions, as observed for crystals and quasicrystals. As a matter of fact, the simplicity of the diffraction pattern depends on the sample symmetry.

When there are two atomic species, there are two independent densities and a similar calculation can be introduced. The generalization of this case to the case with many species is obvious. The general result is obtained when introducing independent variations for each species:

$$\delta n_i(\vec{p}) = C_i \delta(\vec{p} - \vec{p}_0)$$

So one variational equation is obtained for each species:

$$\sum_j n_i(\vec{p}) V_{ij}(\vec{p}) = 0 \tag{9}$$

The special case with two species which can be separated, as it occurs in friction, is of special interest. It provides the system where atomic densities are assumed to be real functions:

$$\begin{aligned} n_I(\vec{p}) V_{I,I}(\vec{p}) + n_{II}(\vec{p}) V_{I,II}(\vec{p}) = 0 \\ n_I(\vec{p}) V_{I,II}(\vec{p}) + n_{II}(\vec{p}) V_{II,II}(\vec{p}) = 0 \end{aligned} \tag{10}$$

These equations show that in the case of a system with a dominant component called I, the atomic density of species I is weakly shifted from a wavevector variation $\delta\vec{p}$ as compared to the case of a pure I material where there is a density peak at wavevector $\vec{p}_1$ to a new wavevector $\vec{p}_1 + \delta\vec{p}$. The difference is given by:

$$n_I(\vec{p}_1 + \delta\vec{p}) \vec{A} * \delta\vec{p} = -n_{II}(\vec{p}_1) V_{I,II}(\vec{p}_1)$$

Where $\vec{A}$ is the gradient of potential $V_{I,I}(\vec{p})$ relative to the wavevector $\vec{p}_1$. This equation means there is an effective pressure in the first material due to

the presence of an extra component, and in first order this pressure varies linearly with the extra content as observed locally for friction [41].

In the general case, the atomic density equation generalizes the one-species equation (5). For instance, for two species, the compatibility of equations (10) means:

$$n_I(\vec{p}_1+\delta\vec{p})\left(V_{I,I}(\vec{p})V_{II,II}(\vec{p})-V^2{}_{I,II}(\vec{p})V_{I,I}(\vec{p})\right)=0 \tag{11}$$

This new equation defines a more complex effective potential energy than individual pair potentials:

$$W(\vec{p})=V_{I,I}(\vec{p})V_{II,II}(\vec{p})-V^2{}_{I,II}(\vec{p})V_{I,I}(\vec{p})$$

And density is non zero only at its nodes.
For any number of species, the compatibility of all equations means:

$$W(\vec{p})=\det\left(V_{i,j}(\vec{p})\right)=0 \tag{12}$$

Once more it defines a new effective potential energy $W(\vec{p})$.

The resolution of equation (12) leads to define a lot of roots $\vec{p}_k$ which are wavevectors. Using a Taylor development of the determinant close to a single root $\vec{p}_k$, leads us to a resolution of density equations (9) which is quite similar to the resolution of equation (5) but with a new wavevector $\vec{p}_k$ resulting from all interactions. Close to this single root, the solution of equation (12) [4, 39] writes:

$$n_i(\vec{p})=C_k\delta(\vec{p}-\vec{p}_k) \tag{13}$$

So finally, the atomic density is a sum of delta-functions in reciprocal space as in equation (6) with new selected wavevectors $\vec{p}_k$ resulting from all interactions as shown in equation (12). As noticed before, this means that the structure factor and the diffraction pattern result from a sum of delta-functions. If the number of terms of the sum is discrete, this diffraction pattern is due to a crystal or a quasicrystal.

In real space, the atomic density of species *i* is a sum of sine waves as in equation (7) with new selected wavevectors resulting from all interactions as shown in equation (12):

$$n_i(\vec{x})=\sum_k C_{i,k}\exp(i\vec{p}_k*\vec{x}) \tag{14}$$

So the next step consists in going from a wavy density function to a discrete density made of wave peaks. Before doing that, it can be shown that

instead of solving this problem by considering directly pair potentials, a more practical solution can be obtained from the observation of an optimal cluster of this material. This is what explains the universality of crystals and quasicrystals, with just a few requirements on the details of pair potentials.

2.3. Generation from a cluster seed

Let us consider an optimal cluster C made of such a material with several components or species. Since C is optimal it fulfils the previous conditions. So this cluster can be considered as the restriction within a box Δ of an optimal structure. So its densities fulfil the condition:

$$n_{i,C}(\vec{x}) = n_i(\vec{x})Y[\Delta]$$

Here $Y(\Delta)$ is the step function of the box Δ. As a matter of fact, with pair potentials, there is a contraction of the optimal distance between atoms and this contraction depends on the sample size. This contraction is practically uniform within the sample, as due to an external pressure [42]. So basically the cluster organization is not changed by this effective extra hydrostatic pressure. So the Fourier transform $F[n_{i,C}]$ of the atomic densities of the cluster C are related to the Fourier transform of the perfect material by a convolution with the Fourier transform of the box Δ when neglecting this contraction:

$$F[n_{i,C}] = F[n_i] \circ F[Y(\Delta)] = n_i(\vec{p}) \circ F[Y(\Delta)] \quad (15)$$

From this convolution the delta peaks of the density $n_i(\vec{p})$ become smoothed for the cluster, with a width π/L where L is the cluster size, and a finite intensity. Reciprocally, this means that the Fourier transforms of a cluster and of an infinite sample are nearly the same, up to these convolution features and the shift due to contraction. Thus it sounds convenient to extract the effective wavevectors $\vec{p}_k$ from the Fourier transform of an optimal cluster C and then to deduce the infinite sample from the Fourier transform of the sum of density waves for these effective wavevectors, up to a uniform contraction or dilation. In such a way, interaction potentials can be forgotten, only their results on a cluster C are accounted for. The main calculation is from the translation from a sum of cosines to a discrete set of points. And this operation occurs twice.

As a matter of fact, between the set of wavevectors $\vec{p}_k$ and the density, there are coefficients $C_{i,k}$. Quite obviously for a symmetric set of wavevectors

$\vec{p}_k$, i.e. invariant under a transformation group, coefficients $C_{i,k}$ must share the same modulus. There is just a phase relation between $C_{i,k}$ which must be consistent with group properties. Here we will take these coefficients $C_{i,k}$ all equal. However different symmetric sets of wavevectors can share the same symmetry, so we will also study this effect.

3. From density to points: 1D density

The transition from a continuous function to a discrete set of points is a classical mathematical problem [43]. Usually the discrete set of extrema of the function defines such a set of points. Here, in the case of density functions, it seems better to define the discrete set of maxima, since maxima lead to a maximum value of the Bragg-Williams interaction (1). But the next question is the practical organization of this set of points. So, a first level of this study consists in looking at 1D densities. This enables us to emphasize an approximate property of **self-similarity** of these sets i.e. of these lattices or quasilattices, and special numeral properties of these similarity ratios. Next, 2D densities with quasicrystalline or crystalline symmetry are considered, and their symmetry properties are again studied.

Our 1D density functions are just linear cuts of full space densities. And here we are considering basically 2D crystals and quasicrystals for the sake of simplicity since the case of icosahedral symmetry is not so different from pentagonal symmetry. So we will introduce the full 2D densities for all the concerned symmetries before considering their 1D cut along x axis, i.e. along a symmetry axis.

3.1. Square seed in reciprocal space, fourfold symmetry

A square of four points on a circle of 2π unit radius is selected in the reciprocal space as a seed and the density function divided by two reads:

$$n_0(x, y) = \cos(2\pi x) + \cos(2\pi y) \tag{16}$$

So the cut along x axis gives simply:

$$f_0(x) = \cos(2\pi x) + 1 \tag{17}$$

This is a periodic function, exactly a sine wave, and its maxima define Z the set of integers, while the maxima of the full 2D density define the set Z^2 which is just the square lattice which has the fourfold symmetry.

3.2. Hexagonal seed in reciprocal space, sixfold symmetry

Six points define the reciprocal hexagon of 2π unit radius and the density function divided by two reads:

$$n_1(x,y) = \cos(2\pi x) + 2\cos(\pi x)\cos\left(\pi y\sqrt{3}\right) \tag{18}$$

The cut along x axis has for density

$$f_1(x) = \cos(2\pi x) + 2\cos(\pi x) \tag{19}$$

This function is periodic with two for period, but within this period there are two maxima, 1 and 2. 1 is the distance between neighbours and 2 is the great diagonal of the hexagon of unit radius. The other diagonal $\sqrt{3}$ appears in the cut off along y axis. Function f_1 is reported in Fig. 1 when x lies in the range [0, 100]. There are two maxima with values 3 and -1. There is also a minimum with the value − 3/2. So the difference between the two maxima is large as seen on Figure 1. And according to selection criterion one or two maxima are selected within the period.

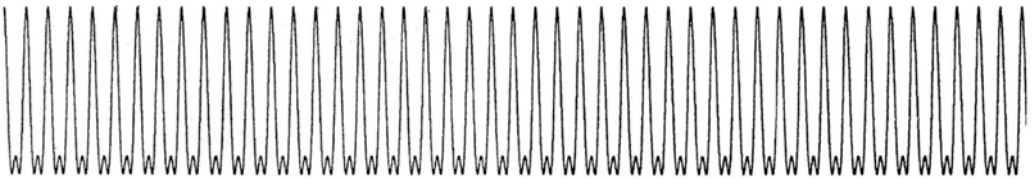

Figure 1. The triangular density function $f_1(x)$ when the coordinate x lies in the range [0, 100]. Levels 0 and 1 are shown by light lines. Note the translational invariance.

3.3. Pentagonal seed in reciprocal space. Decagonal symmetry

A regular pentagon written on a circle of 2π unit radius is selected in reciprocal space. So the density function reads:

$$n_2(x,y) = \cos(2\pi x) + 2\cos(\pi\tau x)\cos\left(2\pi y \sin\left(\frac{4\pi}{5}\right)\right) + 2\cos\left(\frac{\pi x}{\tau}\right)\cos\left(2\pi y \sin\left(\frac{2\pi}{5}\right)\right) \tag{20}$$

Here τ is the golden number: $\tau = 2\cos\left(\frac{\pi}{5}\right) = 1.61803..$ and the other parameters are related to this number.
The cut along x axis has for density

$$f_2(x) = \cos(2\pi x) + 2\cos(\pi\tau x) + 2\cos\left(\frac{\pi x}{\tau}\right) \tag{21}$$

From the previous remark on maxima, numbers n which are close to integer numbers and such as τn and $\frac{n}{\tau} = n(\tau - 1)$ be close to even integer numbers give maxima of f_2. Since τ is an incommensurate number, there is no exact solution for a perfect maximum value. This is the difference with the case of a commensurate ratio.

The golden number τ is a root of the Fibonacci equation: $x^2 - x - 1 = 0$. So the Fibonacci series $u_{n+1} = u_n + u_{n-1}$ defines Fibonnaci integers which fulfil approximately this condition as shown by Binet formula [44]:

$$u_n = \frac{\tau^n - (1-\tau)^n}{\sqrt{5}} \tag{22}$$

So τu_n is quite close from the integer u_{n+1}, and this agreement improves when n increases since $1 - \tau$, the second root of Fibonacci equation has a modulus lower than 1. Binet formula is easily understood from the matrix formulation of Fibonacci series:

$$\begin{pmatrix} u_{n+1} \\ u_n \end{pmatrix} = \begin{pmatrix} 1 & 1 \\ 1 & 0 \end{pmatrix} \begin{pmatrix} u_n \\ u_{n-1} \end{pmatrix} = \mathbf{M} \begin{pmatrix} u_n \\ u_{n-1} \end{pmatrix} = \mathbf{M}^n \begin{pmatrix} u_1 \\ u_0 \end{pmatrix} \tag{23}$$

It defines the Fibonacci matrix : $\mathbf{M} = \begin{pmatrix} 1 & 1 \\ 1 & 0 \end{pmatrix}$

This last property for the Fibonacci equation means that the golden number is a Pisot number since it is a root of an algebraic equation and the only root with modulus larger than one [45]. So the function f_2 reported in Figure 2 is not periodic but quasiperiodic. Binet formula means that there are quite numerous peaks reaching high values. And the quality of these maxima improves when their size increases. So there are good maxima up to infinity.

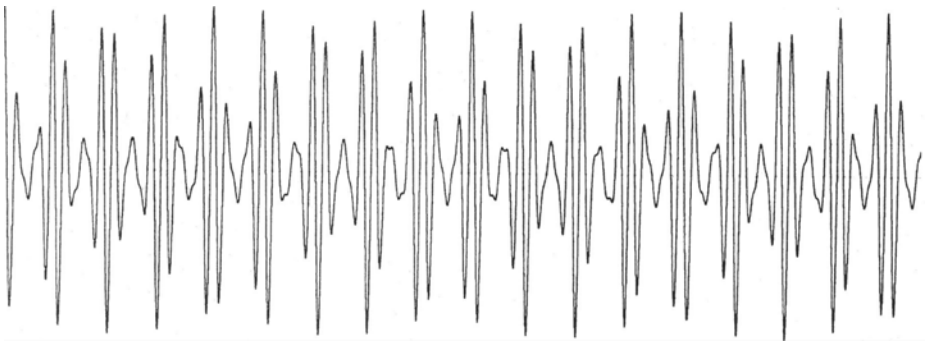

Figure 2. The pentagonal density function f_2 (x) when the coordinate x lies in the range [0, 100]. Note the large number of peaks at rather regular distances.

This ensures the order propagation over the whole plane since there is also an obvious fivefold symmetry for the 2D density $n_2(x, y)$. As before, a geometrical property of this number must be noticed: τ is also the value of the only diagonal of the pentagon of unit side.

It must also be noticed that there is no difference between pentagonal and decagonal symmetry since the density function as defined here is invariant under central symmetry.

3.4. Octagonal seed in reciprocal space, eightfold symmetry

A regular octagon of 2π unit radius in reciprocal space defines the density function $n_3(x, y)$ in real space:

$$n_3(x, y) = 2\cos(2\pi x) + 4\cos\left(\pi x\sqrt{2}\right)\cos\left(\pi y\sqrt{2}\right) + 2\cos(2\pi y) \tag{24}$$

The cut of half this density function along x axis has for density, up to an additive unity:

$$f_3(x) = \cos(2\pi x) + 2\cos\left(\pi x\sqrt{2}\right) \tag{25}$$

As about fivefold symmetry, one can notice here that integers which multiplied by $\sqrt{2}$ are close to an integer give maxima for $f_3(x)$. So the **silver number** $\delta_s = 1 + \sqrt{2}$ which is associated with the algebraic equation $x^2 - 2x - 1 = 0$ defines the **silver series** $v_{n+1} = 2v_n + v_{n-1}$ of integers which satisfy this property. This defines the silver series matrix **M'**:

$$\mathbf{M'} = \begin{pmatrix} 2 & 1 \\ 1 & 0 \end{pmatrix} \tag{26}$$

So the silver series writes:

$$\begin{pmatrix} v_{n+1} \\ v_n \end{pmatrix} = \mathbf{M'}\begin{pmatrix} v_n \\ v_{n-1} \end{pmatrix} = \mathbf{M'}^n \begin{pmatrix} v_1 \\ v_0 \end{pmatrix}$$

And the silver eigenvalues are δ_s and $-\delta_s^{-1}$. Since the silver number is a Pisot number because the second root $-\delta_s^{-1} = 1-\sqrt{2}$ has a modulus lower than unity, the silver series defines better and better maxima for $f_3(x)$ when n is increased. So the function f_3 reported in Figure 3 is not periodic but quasiperiodic. This means that there are quite numerous peaks reaching high values.

Figure 3. The octagonal density function $f_3(x)$ when the coordinate x lies in the range [0, 100]. Note the large number of peaks at rather regular distances.

For a regular octagon of unit radius, the distance between nearest neighbours is $\sqrt{2-\sqrt{2}}$, the smallest diagonal has for length $\sqrt{2}$, and the two other diagonals have for length $\sqrt{2+\sqrt{2}}$ and 2. So the numbers of the silver series are approximate times the small diagonal. That explains the abundance of maxima. The cut along x axis and along y axis are identical. That reinforces the abundance of maxima.

3.5. Dodecagonal seed in reciprocal space, twelvefold symmetry

A regular dodecagon of 2π unit radius in reciprocal space gives the density function:

$$n_4(x,y) = 2\cos(2\pi x) + 4\cos(\pi x)\cos\left(\pi y\sqrt{3}\right) + 4\cos(\pi y)\cos\left(\pi x\sqrt{3}\right) + 2\cos(2\pi y) \quad (27)$$

The cut of half this density function along x axis has for density, up to a unity:

$$f_4(x) = \cos(2\pi x) + 2\cos(\pi x) + 2\cos\left(\pi x\sqrt{3}\right) \quad (28)$$

As before one can notice that integers which multiplied by $\sqrt{3}$ are close to an integer give maxima for $f_4(x)$. So the number $\delta = 2 + \sqrt{3}$ which is associated with the algebraic equation $x^2 - 4x + 1 = 0$ defines the series $w_{n+1} = 4w_n - w_{n-1}$ of integers which satisfy this property. This series can be written in a matrix form with:

$$\begin{pmatrix} w_{n+1} \\ w_n \end{pmatrix} = \begin{pmatrix} 4 & -1 \\ 1 & 0 \end{pmatrix} \begin{pmatrix} w_n \\ w_{n-1} \end{pmatrix} = \mathbf{M}'' \begin{pmatrix} w_n \\ w_{n-1} \end{pmatrix} = \mathbf{M}''^n \begin{pmatrix} w_1 \\ w_0 \end{pmatrix} \quad (29)$$

Since the number δ is a Pisot number because the second root $2 - \sqrt{3} = \delta^{-1} = 4 - \delta$ has a modulus lower than unity, this series defines better and better maxima for $f_4(x)$ when n is increased. So the function f_4 reported in Figure 4

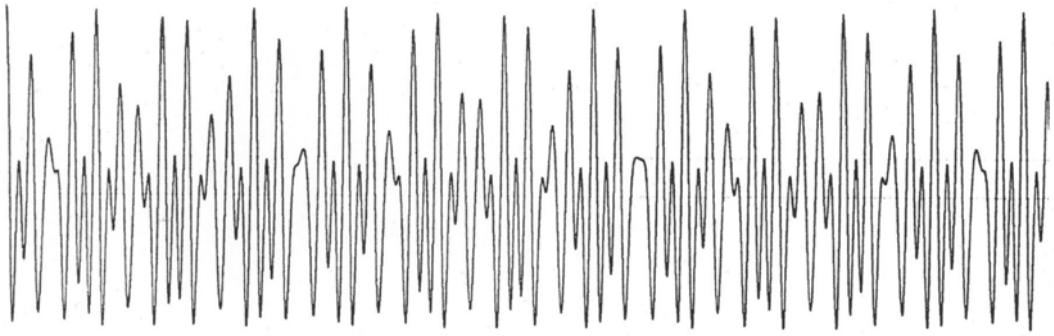

Figure 4. The dodecagonal density function $f_4(x)$ when the coordinate x lies in the range [0, 100]. Note the large number of peaks at rather regular distances.

is not periodic but quasiperiodic. This means that there are quite numerous peaks reaching high values. And this occurs up to infinity. About the regular dodecagon geometry with a unit radius, it must be noticed that the nearest neighbour distance is equal to: $\sqrt{2-\sqrt{3}}=\sqrt{4-\sqrt{\delta}}$, and that the first diagonals have for length $1, \sqrt{2}$, $\sqrt{3}=\delta$-2, $\sqrt{2+\sqrt{3}}=\sqrt{\delta}$ and 2 respectively. This ensures that the δ series contains several diagonals, thus figures issued from dodecagons can be arranged in order to obtain maxima.

It is of interest to compare this case issued from a dodecagonal seed in reciprocal space, with the one issued from a double dodecagon in reciprocal space, made from twelve rhombi with unit side, this is the case n'_4 (x, y) and with the one issued from a triple dodecagon with twelve more rhombi with unit side, this is the case n''_4 (x, y). This comparison will enable us to see if different quasicrystalline structures with the same symmetry can be defined. They have for half densities, respectively:

$$\begin{aligned} n'_4(x,y) &= \cos(2\pi x)+2\cos(\pi x)\cos\left(\pi y\sqrt{3}\right)+2\cos(\pi y)\cos\left(\pi x\sqrt{3}\right)+\cos(2\pi y) \\ &+2\cos(2\pi x)\cos\left(2\pi y\left(2+\sqrt{3}\right)\right)+2\cos(2\pi y)\cos\left(2\pi x\left(2+\sqrt{3}\right)\right)+2\cos\left(2\pi x\left(1+\sqrt{3}\right)\right)\cos\left(2\pi y\left(1+\sqrt{3}\right)\right) \end{aligned} \quad (30)$$

And

$$\begin{aligned} n''_4(x,y) &= \cos(2\pi x)+2\cos(\pi x)\cos\left(\pi y\sqrt{3}\right)+2\cos(\pi y)\cos\left(\pi x\sqrt{3}\right)+\cos(2\pi y) \\ &+2\cos(2\pi x)\cos\left(2\pi y\left(2+\sqrt{3}\right)\right)+2\cos(2\pi y)\cos\left(2\pi x\left(2+\sqrt{3}\right)\right)+2\cos\left(2\pi x\left(1+\sqrt{3}\right)\right)\cos\left(2\pi y\left(1+\sqrt{3}\right)\right) \\ &+2\cos\left(\pi x\left(1+\sqrt{3}\right)\right)\cos\left(\pi y\left(3+\sqrt{3}\right)\right)+2\cos\left(\pi x\left(3+\sqrt{3}\right)\right)\cos\left(\pi y\left(1+\sqrt{3}\right)\right) \\ &+\cos\left(2\pi x\left(1+\sqrt{3}\right)\right)+\cos\left(2\pi y\left(1+\sqrt{3}\right)\right) \end{aligned} \quad (31)$$

The main point to notice is that these new densities which are more complex than n_4 share with it the same maxima for the cut along x axis, since integers which multiplied by $\sqrt{3}$ have an integer value define also maxima for these

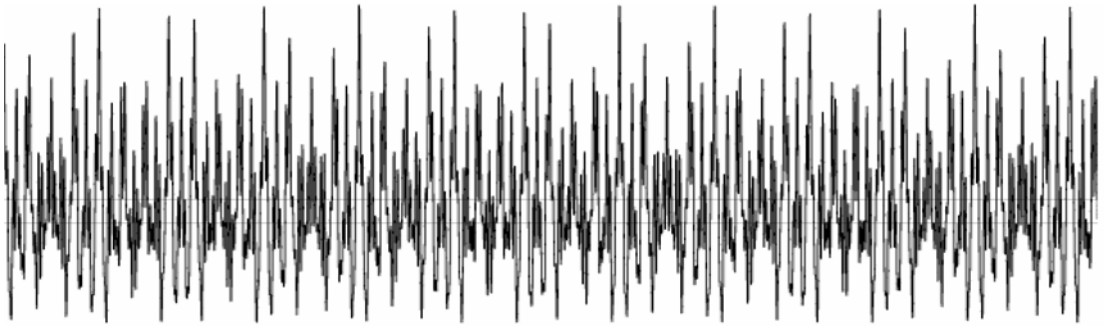

Figure 5. The dodecagonal density function $f_4^{'}(x)$ when the coordinate x lies in the range [0, 100]. Levels 1 and 0 are marked by a light line. Note the reduced number of well isolated peaks as compared to those in Figure 4.

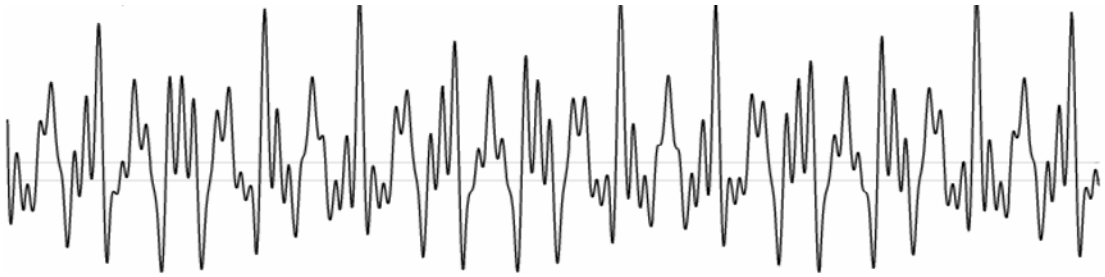

Figure 6. The dodecagonal density function $f_4^{''}(x)$ when the coordinate x lies in the range [0, 100]. Levels 1 and 0 are marked by a light line. Note the quite reduced number of peaks as compared to those in Figure 4.

functions. And this property is the characteristic of this δ series. But the corresponding maximum values are not comparable for the three samples. This is well observed in Figures 5 and 6 when compared to Figure 4.

Quite obviously the structures described by the respective densities $n_4(x, y)$, n'_4 (x, y) and n''_4 (x, y) are quite different even if they share the same symmetry and the same self similarity with a large number of peaks.

3.6. Heptagonal seed in reciprocal space, sevenfold symmetry

A regular heptagon of 2π unit radius in reciprocal space gives the density function:

$$n_5(x,y) = \cos(2\pi x) + 2\cos\left(\pi x\cos\left(\frac{2\pi}{7}\right)\right)\cos\left(\pi y\sin\left(\frac{2\pi}{7}\right)\right)$$
$$+ 2\cos\left(\pi x\cos\left(\frac{4\pi}{7}\right)\right)\cos\left(\pi y\sin\left(\frac{4\pi}{7}\right)\right) + 2\cos\left(\pi x\cos\left(\frac{6\pi}{7}\right)\right)\cos\left(\pi y\sin\left(\frac{6\pi}{7}\right)\right) \qquad (32)$$

The cut of this density function along x axis has for density:

$$f_5(x) = \cos(2\pi x) + 2\cos\left(\pi x \cos\frac{2\pi}{7}\right) + 2\cos\left(\pi x \cos\frac{4\pi}{7}\right) + 2\cos\left(\pi x \cos\frac{6\pi}{7}\right) \tag{33}$$

So three non integers appear, they are linked with the heptagon diagonals which are deduced from the roots of unity:

$$x^7 - 1 = 0$$

This is done by means of the transformation $u = x + \frac{1}{x}$ where the lengths of diagonals appear as roots of :

$$u^3 + u^2 - 2u - 1 = 0. \tag{34}$$

These roots are: $2\cos\left(\frac{2\pi}{7}\right) = 1.247..,\ 2\cos\left(\frac{4\pi}{7}\right) = -0.445..,\ 2\cos\left(\frac{6\pi}{7}\right) = -1..802....$

These roots are also the eigenvalues of the characteristic matrix **Z** of this series which is defined in a matrix way by:

$$\begin{pmatrix} z_{n+1} \\ z_n \\ z_{n-1} \end{pmatrix} = \mathbf{Z}\begin{pmatrix} z_n \\ z_{n-1} \\ z_{n-2} \end{pmatrix} = \begin{pmatrix} -1 & 2 & 1 \\ 1 & 0 & 0 \\ 0 & 1 & 0 \end{pmatrix}\begin{pmatrix} z_n \\ z_{n-1} \\ z_{n-2} \end{pmatrix} = \mathbf{Z}^{n-1}\begin{pmatrix} z_2 \\ z_1 \\ z_0 \end{pmatrix} \tag{35}$$

So equation (34) is not a Pisot equation [45]. And very large integer values are required in order to obtain a good maximum for the densities n_5 and f_5. As a consequence, the function f_5 has just a few maxima in the range [0,100] as seen on Figure 7. And there is no regular order in these maxima.

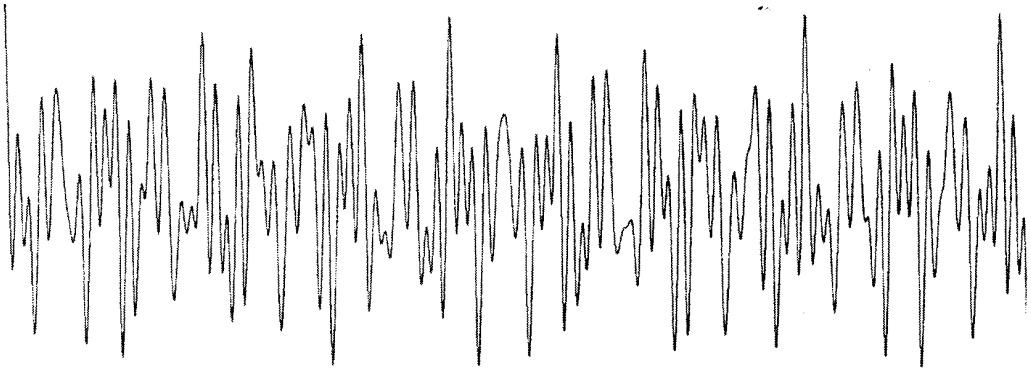

Figure 7. The heptagonal density function f_5 (x) when the coordinate x lies in the range [0, 100]. Note the low number of peaks at rather irregular distances.

3.7. Elevenfold seed in reciprocal space. Elevenfold symmetry

A regular polygon with eleven sides on a circle of 2π unit radius in reciprocal space gives the real density function:

$$n_6(x,y)=\cos(2\pi x)+2\cos\left[2\pi x\cos\frac{2\pi}{11}+2\pi y\sin\frac{2\pi}{11}\right]+2\cos\left[2\pi x\cos\frac{4\pi}{11}+2\pi y\sin\frac{4\pi}{11}\right]$$
$$+2\cos\left[2\pi x\cos\frac{6\pi}{11}+2\pi y\sin\frac{6\pi}{11}\right]+2\cos\left[2\pi x\cos\frac{8\pi}{11}+2\pi y\sin\frac{8\pi}{11}\right]$$
$$+2\cos\left[2\pi x\cos\frac{10\pi}{11}+2\pi y\sin\frac{10\pi}{11}\right] \qquad (36)$$

And the x axis cut is easily defined:

$$f_6(x)=\cos(2\pi x)+2\cos\left(2\pi x\cos\frac{2\pi}{11}\right)+2\cos\left(2\pi x\cos\frac{4\pi}{11}\right)+$$
$$2\cos\left(2\pi x\cos\frac{6\pi}{11}\right)+2\cos\left(2\pi x\cos\frac{8\pi}{11}\right)+2\cos\left(2\pi x\cos\frac{10\pi}{11}\right) \qquad (37)$$

As before this defines an equation for the five different diagonals of this polygon:

$$u^5+u^4-4u^3-3u^2+3u+1=0 \qquad (38)$$

With the lengths:

$$2\cos\left(\frac{2\pi}{11}\right)=1.682,\quad 2\cos\left(\frac{4\pi}{11}\right)=0.831,\quad 2\cos\left(\frac{6\pi}{11}\right)=-0.285,$$
$$2\cos\left(\frac{8\pi}{11}\right)=-1.31,\quad 2\cos\left(\frac{10\pi}{11}\right)=-1.919$$

Three diagonals of this polygon have a length larger than unity. So equation (38) is not a Pisot equation [45]. Of course equation (38) could be used to define a series of integer numbers, but these numbers multiplied by one of these roots are not necessarily close to an integer. So very large integer values for the variable x are required in order to fulfil the conditions for obtaining a good maximum of f_6. And this research can be done only by means of trial and error process. As a conclusion the function f_6 has just a few maxima in the range [0,100] as seen on Figure 8, and there is no hope for obtaining a better situation on a larger range. So the structure deduced from density n_6 does not give a stable quasicrystal.

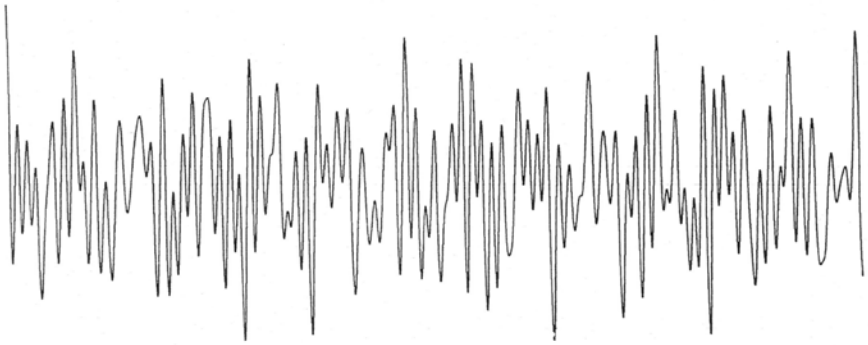

Figure 8. The elevenfold density function f_6 as a function of coordinate x in the range [0,100]. Note that peaks are not regularly spaced in comparison with Figs. 1–4.

As a conclusion of this study of 1D densities, the square symmetry and the hexagonal symmetry are compatible with translation. They define crystalline structures. Pentagonal symmetry, octagonal symmetry and dodecagonal symmetry define rather dense sets of maxima, so they are good candidates to be nearly as stable as crystals. Within this class, the octagonal symmetry is the best structure as defined by its 1D cut. The introduction of more complex seeds in reciprocal space leads to different structures as seen for dodecagonal symmetry. The 1D density for sevenfold symmetry as well as the one for elevenfold symmetry are quite noisy and thus are not expected to lead to stable structures. In the cases of stable quasicrystals approximate self similarity is found. But the ratios of these self similarities are not rational, there are algebraic numbers, and the stability of the corresponding structures depends on the algebraic properties of these numbers. With a Pisot number for similarity ratio as it occurs, a large number of regularly classified maxima of the 1D density appears.

4. 2D density and quasicrystals

The derivation of 2D crystals, simple square and triangular, is obvious, so it is omitted in this paper.

4.1. Pentagonal or decagonal symmetry

Equation (20) gives us the 2D density which is reported in Figure 9a in the range [(0,10), (0,10)] and in Figures 9b,c in the range [(−5,5), (−5,5)].

These level curves could be easily extended over large ranges. And these level curves are quite similar to those obtained from superposed waves [12]. The density maxima are easily defined. These maxima exhibit different shapes:

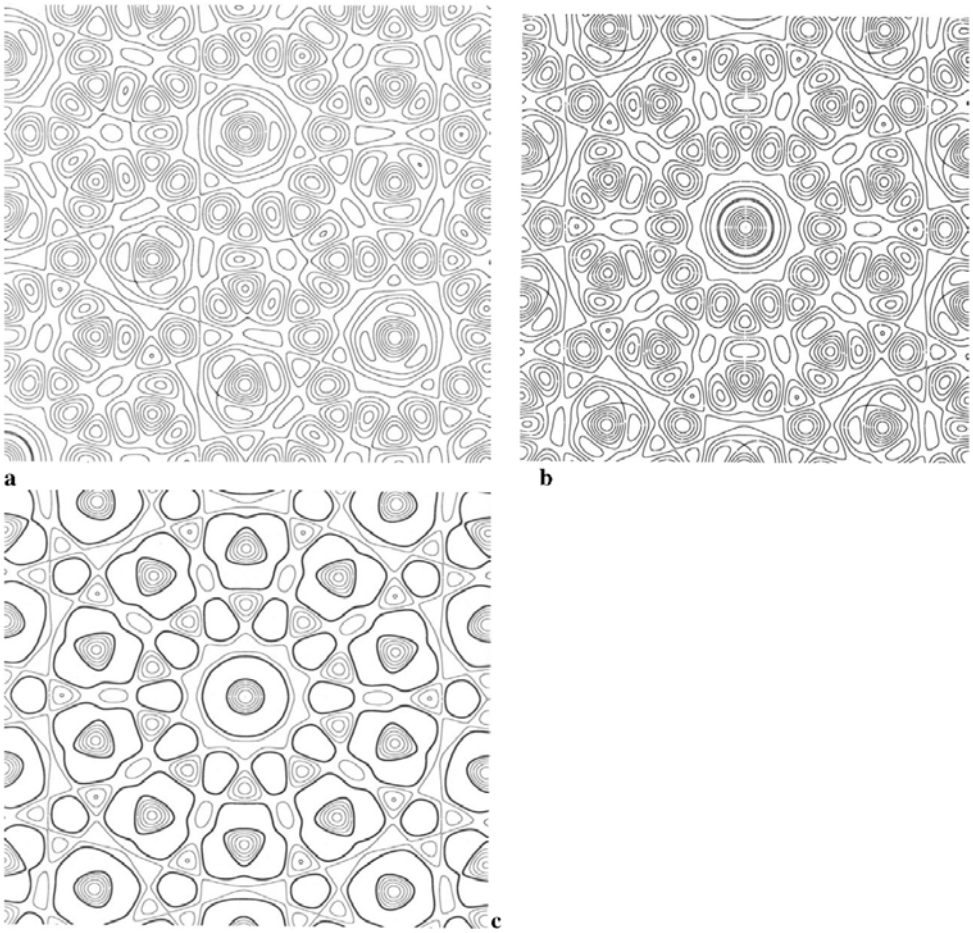

Figure 9. The level map of the quasicrystalline density function n_1 : integer levels are shown, a) in the range [(0,10), (0,10)], b) in the range [(−5,5), (−5,5)], c) only positive levels are shown in the range [(−5,5), (−5,5)].

conic with a circular basis or with two or three faces and so on. Some of these maxima are rather flat at least in one direction. The distances between maxima are discrete. A first peak in the pair distribution function appears at a value $0.6 \cong \tau^{-1}$. This enables us to represent on the same graph, Figure 10, the level map within the range [(−10,10), (− 10,10)], the set of maxima as points and the links of length $0.6 \cong \tau^{-1}$ between maxima.

Links with next nearest neighbour inter-distances were plotted in a similar work [46], with the appearance of another tiling. The tiling which appears in Figure 10 is made of numerous tiles. And this tiling percolates through the 2D plane. It contains a few Penrose rhombi and a lot of decagons of various shapes. It can be noticed that these decagons or polygons with twenty sides can be cut in smaller units if a larger range is admitted for

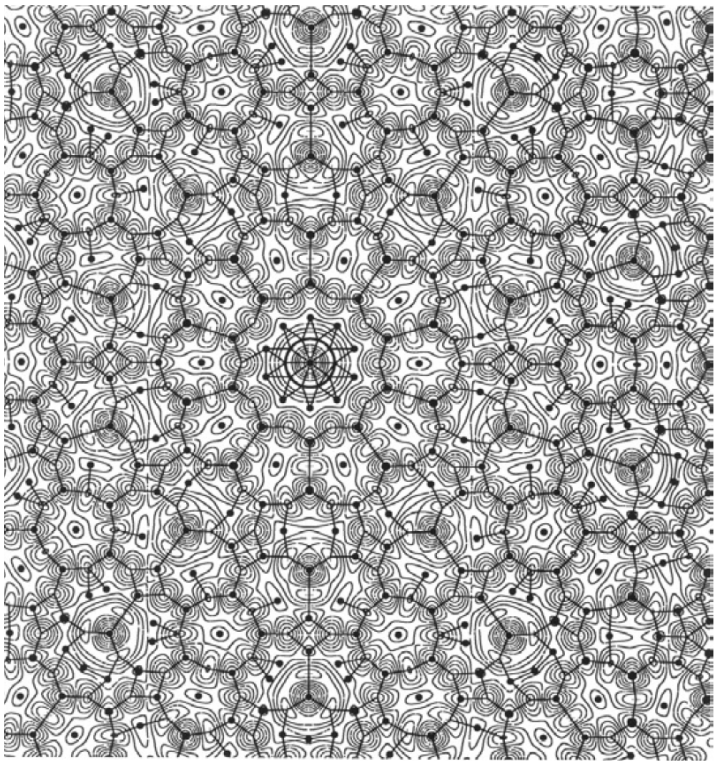

Figure 10. The level map of the quasicrystalline density function n_1 in the range [(-10,10), (-10,10)], the set of maxima as bold points and the set of links between maxima distant from 0.6 as bold bonds. Numerous local figures are evidenced.

defining lengths. Among the polygons with a large number of sides, numerous dead branches, i.e. dead links are observed. There is a choice in the sharpness of the definition of the link length, and the present choice is rather optimized. The structure plotted in figure 10 is comparable with the best high resolution electron microscope 2D image of quasicrystals with icosahedral symmetry [47]. The observation with atomic resolution Z contrast of AlNiCo decagonal quasicrystals [48] confirms the existence of several shapes of decagons.

From the observation of the level maps of Figures 9 and 10 it is obvious that all points are not defined with the same level of consistency. This was already true about the 1D density curve of Figure 2. As a consequence some maxima can be either unoccupied sites or shifted sites, as it is easily produced in the case of a flat maximum. This generalizes the notion of vacancy and interstitial site in crystals. It defines here **local defects**. The shift from one maximum site to a lower maximum site close to it defines an atomic motion which can be restricted to a very few atomic sites, as studied during relaxation [26-27]. This is called a **phason** state [49] as for commensurate

and incommensurate structures [50] where similar properties of abundant maxima occur. These phasons differ from phonons in that there are rather **localized**, independently from the sample shape, while localized phonons are just localized close to the external parts.

As already observed about 1D density, there is a classification of maxima according to their values. As noticed about Fibonacci series, the best density maxima are the farthest. Because of the tenfold effective symmetry, this means a very large decagon of best maxima. The next maxima define also a decagon, with a smaller size. And the Fibonacci series proves that the similarity ratio between these decagons is close to the golden number τ. So there is a natural self similarity between successive density maxima. Since regular pentagons can be cut into two flat triangles, kites according to Penrose's labelling, and one sharp triangle, dart according to Penrose's labelling, and that darts and kites can be cut themselves in another step into self similar darts and kites with τ for similarity ratio, this self similarity has a real 2D meaning, at least approximately. About Penrose's and Robinson's tilings, this self similarity among a family of triangles defines **correction** dimensions, and some of them are complex [51]. These complex correction dimensions correspond to the fact that a triangle of this family does not produce itself at the next iteration step, but several steps are required to produce the same triangle. This means the occurrence of similar maxima at rather large distances from each other for these quasicrystals with decagonal symmetry. So there is a strong connection between this so **frustrated** self similarity of quasicrystals with decagonal symmetry and the existence of phasons in such structures since this long ranged correlation can admit some fluctuations in this order. This geometric frustration is characteristic of quasicrystals as it occurs for other quasicrystals too.

4.2. Octagonal symmetry

Equation (23) gives us the 2D density function for this octagonal symmetry. And the level curves of this density are reported in Figure 11a and b in the range [(−5,5), (−5,5)]. In figure 11a all integer levels are shown, while in figure 11 b only positive integer levels are shown.

These level curves are easily extended over larger ranges. And the results are quite similar to those obtained from superposed waves [12]. The density maxima are easily defined. They exhibit different shapes, from perfect sharp cones with circular basis to flat cliffs, with also facetted peaks. The distances between maxima are discrete. A first peak in the pair distribution function of maxima appears at a value $\sqrt{2}$, as expected from the previous arguments which lead us to introduce the silver number and the silver series. Links of this

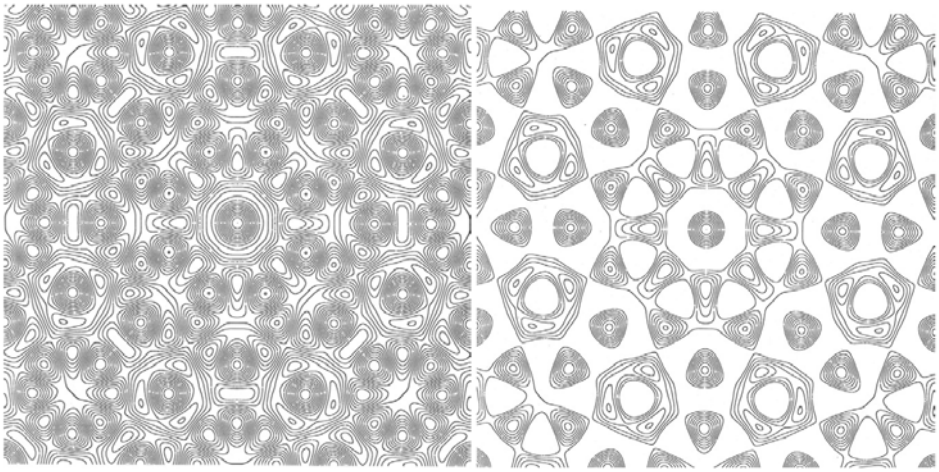

Figure 11. The level curves of the density function $n_3(x, y)$ in the range [−5,5), (−5,5)], with a) all integer levels, b) all positive integer levels.

length $\sqrt{2}$ connect sites and form octagons and a few segments [52]. The next peak in the pair distribution function occurs at the distance $\sqrt{2+\sqrt{2}} \cong 1.85$ which has been already noticed to be a diagonal length of the octagon. The set of these links or bonds between maxima percolates through the 2D plane, with the appearance of numerous squares and 45° rhombi. This enables us to represent on Figure 12 the set of maxima as points and the links of length $\sqrt{2+\sqrt{2}} \cong 1.85$ between maxima within the range $r < 16.8$. This perfect construction is easily extended to contain several thousands of maxima [52]. One recognizes exactly the Ammam-Beenker tiling [15] made of squares and 45° rhombi, up to boundary effects. This model is used as a basis for understanding experimental observations on octagonal quasicrystals [53]. This observation means that basic rhombi and squares are decorated with a few atoms.

As before it must be noticed that the information on maxima can be used to define defects and low energy motions. In the part shown in Figure 11b, there is no unoccupied maximum. So there are not so many defects in the whole sample. Yet some maxima are rather flat according to some directions. Since there are different shapes for these maxima, there are different modes for these displacements. This defines low energy phasons.

The values of the maxima can be classified. This is clearly seen from Figure 3 and equations (24) and (25). Along a central axis, this classification occurs according to the silver series, so there is a natural self similarity ratio which is the silver number $\delta_S = 1+\sqrt{2}$. This defines self similar octagons. It must be noticed from Figures 11 and 12 that such a self similar ratio transforms a square of Figure 12 into a larger square which contains 4 small

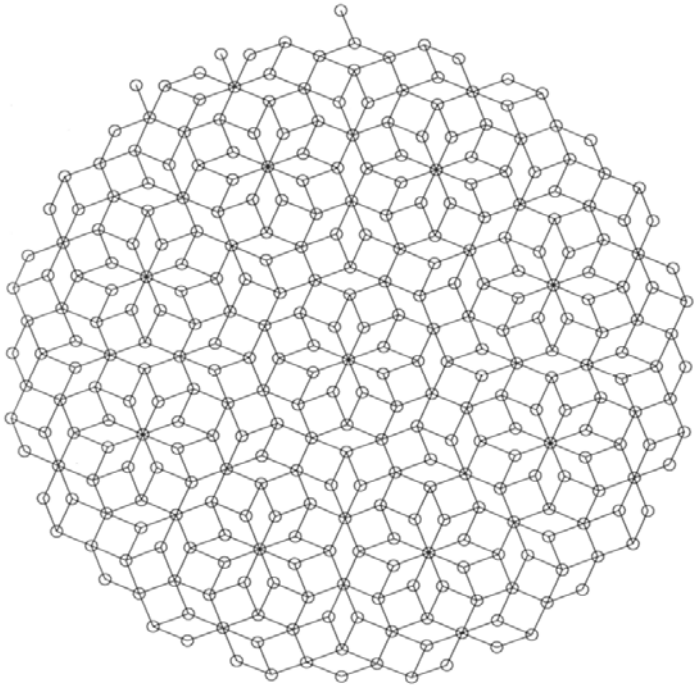

Figure 12. The extrema of the quasicrystalline density function $n_3(x, y)$ with eightfold symmetry when $r < 16.8$ are shown by circles. Links between maxima located at a distance $\sqrt{2+\sqrt{2}} \cong 1.85$ are shown by segments. Note the regular Ammam-Beenker tiling.

rhombi and 3 small squares. Similarly a large rhombus contains 3 small rhombi and 2 small squares. This defines a similarity matrix **T** :

$$\begin{pmatrix} R \\ S \end{pmatrix} = \begin{pmatrix} 3 & 2 \\ 4 & 3 \end{pmatrix} \begin{pmatrix} r \\ s \end{pmatrix} = \mathbf{T} \begin{pmatrix} r \\ s \end{pmatrix} \tag{39}$$

And this similarity matrix has for eigenvalues $\delta_S{}^2 = 3 + 2\sqrt{2}$ and $\delta_S{}^{-2} = 3 - 2\sqrt{2}$. Of course the square shown in these eigenvalues is due to the 2D dimensions of the plane. These eigenvalues must be compared to the eigenvalues of the 1D self similarity matrix which is the silver number matrix **M'** with eigenvalues: δ_S and $-\delta_S{}^{-1}$. So there is a natural link between the construction by the energy method and the construction by self-similarity.

4.3. Dodecagonal symmetry

Here from equations (27-29), the dodecagonal series is defined from the dodecagonal matrix **M"** as defined in equation (29):

$$\mathbf{M}'' = \begin{pmatrix} 4 & -1 \\ 1 & 0 \end{pmatrix} \tag{40}$$

This matrix has two eigenvalues $\delta = 2+\sqrt{3}$ and $\delta^{-1} = 2-\sqrt{3}$. So as in the previous cases of pentagonal and octagonal symmetry only one eigenvalue has a modulus larger than unity, so the quality of the maximum on axis x for instance improves continuously when the series number is increased, as shown from equation (29) and from the corresponding Binet's formula about decagonal quasicrystals. This remark together with the dodecagonal symmetry defines an overall self similarity of the density functions with dodecagonal symmetry.

In this case we introduce three different models of density issued from three different seeds in reciprocal space. So the comparison between these different densities which share the same self similarity is interesting. It must be said that for a single species, there is probably just one node of the pair potential in reciprocal space, so just equation (27) is fully justified. For the other cases with several values of the potential nodes in Fourier space, the agreement with effective pair potentials for different species must be checked.

So as before, the density levels, the position of maxima and the main links between maxima are reported for each density function. In order to introduce this point, level curves of the density function n_4 (x, y) are reported in Figure 13 for all integer levels in the range $x \in [-5,5]$, $y \in [-5,5]$. It must be

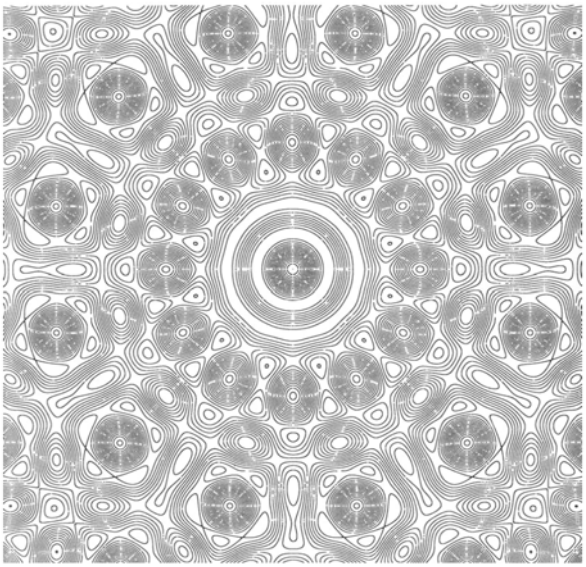

Figure 13. The level curves of the density function $n_4(x, y)$ in the range [(–5,5)(–5,5)], all integer levels are shown. Note the different shapes of maxima, and thus the occurrence of phasons.

noticed that some peaks are very well defined while other extrema are less accurate.

Figures 14-17 report level curves, maxima and links for the density functions $n_4(x, y)$, $n'_4(x, y)$ and $n''_4(x, y)$ for comparison. For clarity maxima and links are reported only on the right part of the Figure. Figure 14 reports for

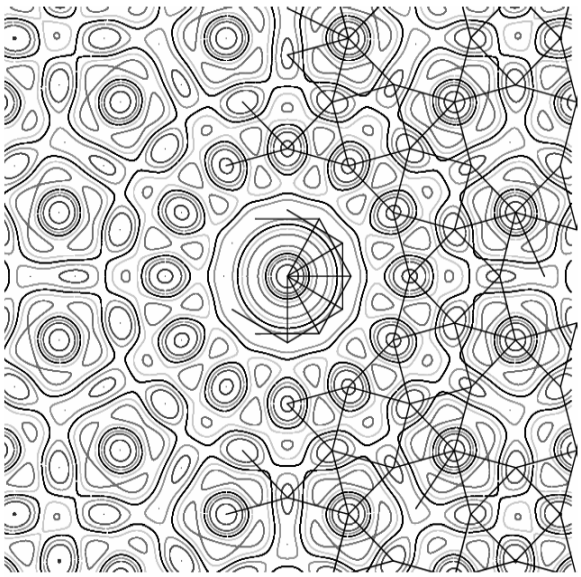

Figure 14. Density levels for $n_4(x, y)$, $x, y \in [-5,5]$, maxima and links for $x \in [0,5]$.

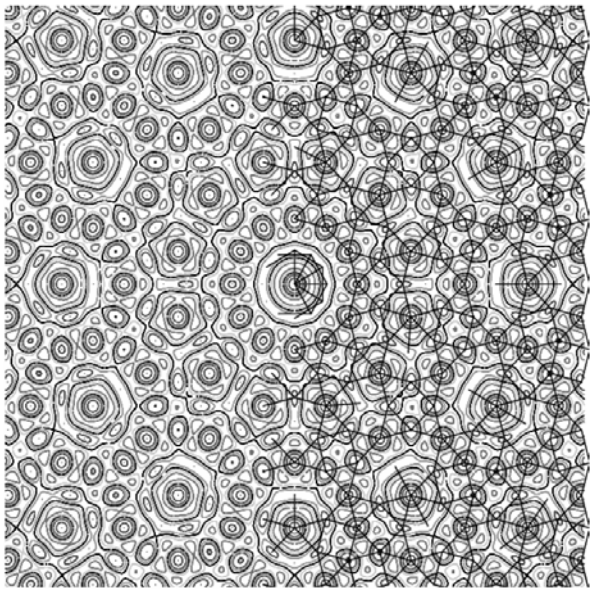

Figure 15. Density levels for $n_4(x, y)$, $x, y \in [-10,10]$, maxima and links for $x \in [0,10]$. On line red =+4, pink=+2, orange=+1, black=0, sky blue=-1, dark blue=-2. On paper grey levels are seen.

$n_4(x, y)$, in the same range as in Figure 13 but with different colours: red (+4) pink (+2) orange (+1) black (0) sky blue (-1) and dark blue (- 2) on line and with different grey levels on paper. Maxima and links at distance 1.14, deduced from the pair distribution function, are shown as superimposed on the density levels on the right part. That reveals a complex structure of bonds made of squares, equilateral triangles, shared dodecagons, pending bonds, which obviously percolates through the 2D plane. This structure is more complex than the octagonal Ammam-Beenker quasicrystal found previously. It contains several well identified forms. Figure 15 extends the range to $[(-10,10)(-10,10)]$.

As about previous Figures on quasicrystals, different shapes of maxima are observed. This defines different **phason** modes since different atomic motions can be defined. From the general self similarity which was pointed out, very well defined peaks occur at the larger dodecagon of the series. This ensures a strong **localization** to these numerous phason modes since these well defined maxima pin the atomic displacements. This is clearly seen when comparing Figures 14 and 15. In Figure 15 there are high level maxima which could be practically considered as centres of a quasicrystalline dodecagonal structure, so defining secondary peaks.

The introduction of different seeds with the same symmetry in the reciprocal space does not change the self similarity properties, but changes significantly the density as shown in the 1D density of Figures 4-6. Of course this observation means that there are also large 2D density changes in Figures 16 and 17 compared to Figure 15 as it can be checked. About maxima it means that between successive central dodecagons very well defined in all these Figures, there are significant changes in what can be called decorative atoms. In Figures 14 to 17 the same link length 1.14 between connected maxima is used. Yet in Figure 16 there is an evidence for a lace made with a radial density oscillation from central dense places to a less dense ring, and then to a dense ring followed by a poor ring and so on. In Figure 17, the density is low nearly everywhere. The shapes of the tiles of Figures 14-17 are basically the same. The density differences between Figures 15-17 are due to a change in the frequency of tiles. In Figure 17, large tiles with a central void are more frequent than in other Figures. A consequence of this low density for more complex seeds is obviously the increase in number of low frequency phasons since in less dense samples, there is less connection, so sites move more easily.

Such a density difference also occurs for crystals deduced from different seeds with the same symmetry. For instance simple cubic, face centred cubic and body centred cubic crystals are issued from seeds with the same symmetry. However in simple cubic lattice each site has six nearest neighbours, in face

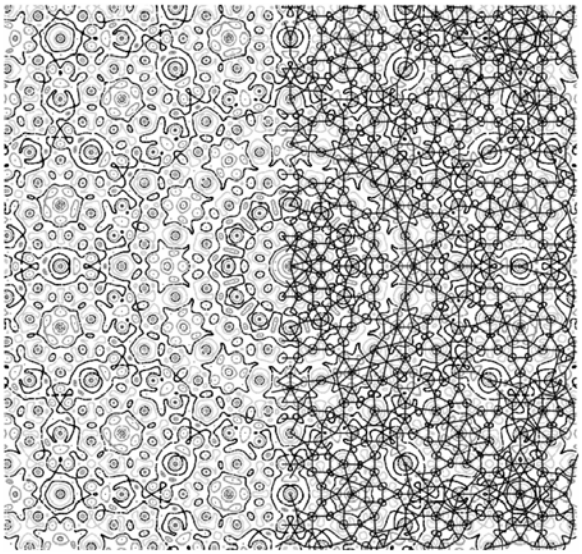

Figure 16. Density levels, for $n'_4(x, y)$, $x, y \in [-10,10]$, maxima and links for $x \in [0,10]$. On line red =+10, pink=+7, orange=+3, black=0, sky blue=-3, dark blue=-10. On paper grey levels are seen.

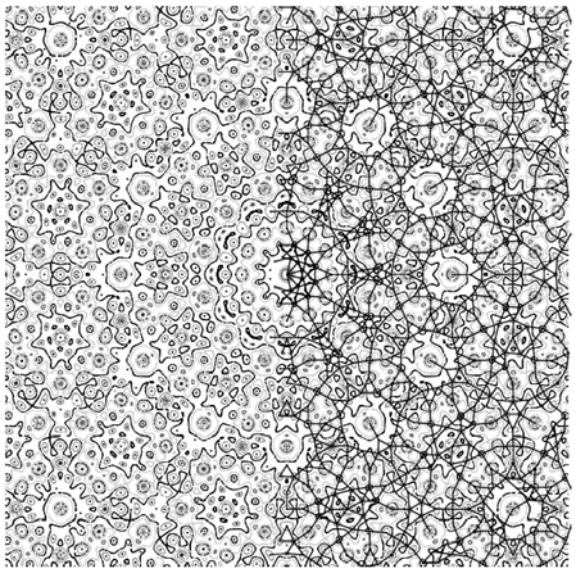

Figure 17. Density levels for $n''_4(x, y)$ $x, y \in [-10,10]$, maxima and links for $x \in [0,10]$. On line red =+10, pink=+7, orange=+3, black=0, sky blue=-3, dark blue=-10. On paper grey levels are seen.

centred cubic lattice each site has twelve nearest neighbours, and in body centred cubic lattice each site has six nearest neighbours and eight close nearest neighbours. As a matter of fact, the most frequent crystals are the densest, face centred cubic, i.e. the crystals with the highest connectivity.

A similar feature can be assumed for quasicrystals. Yet with the use of decorative atoms the difference between the different densities $n_4(x, y)$, $n'_4(x, y)$ and $n''_4(x, y)$ gets smeared out.

Of course for these crystalline samples with different densities, mechanical properties as well as properties of electrical conductivity are different. Because of practical atomic decoration each case must be considered individually.

4.4. Heptagonal symmetry or sevenfold symmetry

Since from equation (35) there is no convergence towards the roots of equation (34), there are only a few heptagons of well defined maxima, and these heptagons are not easily classified. Thus there is no real self similarity between the maxima which can be defined from density $n_5(x, y)$. So trials to define sets of maxima for this density strongly depend on the maximum value introduced and lead to quite inhomogeneous results as shown in Figure 18 of a previous paper [46]. So there is no hope to stabilize such a structure under realistic interactions.

4.5. Elevenfold symmetry

Among the roots of equation (38), three have a modulus larger than one so there is no convergence for the series which can be deduced from this equation. So there is no self similar rule for defining maxima of density $n_6(x, y)$. As a consequence there are only a few regular polygons with eleven sides of well defined maxima, and these polygons are not easily classified. So trials to define sets of maxima for this density strongly depend on the maximum value introduced and lead to quite inhomogeneous results as shown in Figure 19 of a previous paper [46]. So there is no hope to stabilize such a structure under realistic interactions.

5. Diffraction patterns

The diffraction patterns of these set of maxima are easily calculated from the intensity equation:

$$I(\vec{q}) = \left| \sum_i \exp(i\vec{q} \bullet \vec{x}_i) \right|^2 \tag{41}$$

The important property is the self similarity property for operation g with a ratio λ and a rotation ϑ in the plane. Let us introduce the conjugate self

similarity g^* in the reciprocal space with a ratio λ^{-1} and a rotation $-\vartheta$ in the plane. So

$$\vec{q} \bullet \vec{x}_i = g^*(\vec{q}) \bullet g(\vec{x}_i) \tag{42}$$

As a consequence of this property the diffraction pattern is also invariant by self similarity:

$$I(\vec{q}) = I\left(g^*(\vec{q})\right) \tag{43}$$

Thus for the considered quasicrystals which are invariant under self similar operations, their diffraction patterns are also self similar. And as studied before all real quasicrystals exhibit self similar properties. This is the case for tenfold symmetry, for eightfold symmetry and for twelvefold symmetry which have all self similar diffraction patterns. Here for the sake of simplicity we restrict the shown Figures to the case of octagonal symmetry when taking into account 5869 sites found within a disk of radius 75. This case is shown in Figure 18 when introducing different sizes of diffraction points according to the level of the intensity function.

The self similar argument shows that an accurate diffraction pattern requires a very large sample in real space to be considered in order to obtain a good definition. The result shown in Figure 18 is in good agreement with experimental observations [53-56]. As already noticed about sets of maxima

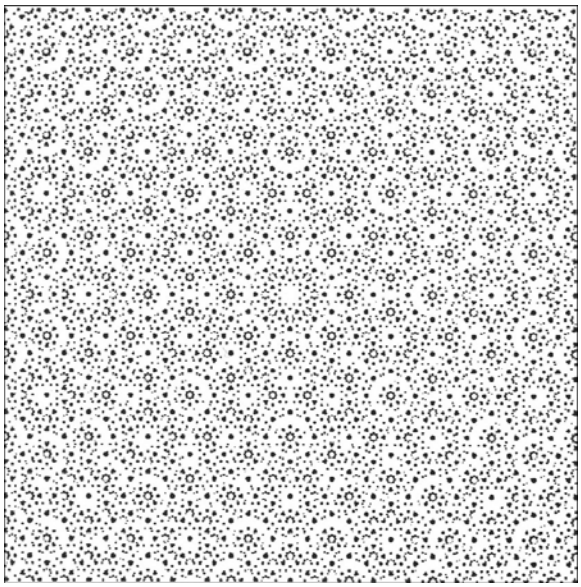

Figure 18. Diffraction pattern of 5869 maxima of the octagonal density n_3 (x, y) within a disk of radius 75: different intensity levels are shown.

of different symmetry, secondary lines, i.e. lines not passing through the origin, also appear in the diffraction pattern and define also tiling properties. This is a general property of quasicrystal diffraction patterns since it is also observed for other quasicrystalline symmetry.

6. Conclusion

This Landau like energetic method of construction of quasicrystalline structures enabled us to build several quasicrystalline structures and to test their stability from simple criteria. As a matter of fact this method can also be used to create defects, i.e. vacancies, in a selected way by assuming a threshold for maxima to be retained. This method, quite obvious in its principle, was used in previous papers to build defected samples [46, 52]. So this method can be used to evaluate the occurrence of defects and thus to calculate the entropy of such systems. About defects and possible motions such as phasons and phonons, this method reveals the non uniformity of sites, not only for the peak values but also for the peak shapes, i.e. for dynamic properties as also revealed by magnetic properties which are sensitive to environments [37]. The self similar properties of quasicrystals lead also to the opening of large band gaps in the acoustic spectrum as in phononic samples [57]. Another property which is shown when using this method is the occurrence of several possible structures with the same overall quasicrystalline symmetry as shown here in the case of quasicrystals with twelvefold symmetry.

Even if more realistic models must be considered with complete interactions, this model shows the complexity of elasticity and mechanics in quasicrystals with the definition of a local "quasicrystalline" field which is not uniform for all sites and the appearance of pinning centres in the quasilattice. These properties are also basic for electrical conductivity.

This energetic method and its result well explain the continuity between the observation of static quasicrystalline structures and the observation of dynamic superposition of waves [12]. Finally the preparation and observation of nano-quasicrystalline phases [58] opens new ways for such studies in the nano-world.

References

1. P. Duwez and S. C. H. Lin, J. Appl. Phys. **38**, 4096 (1967); P. Duwez, J. Vac. Sci. T. B, **1**, 218 (1983).
2. See for instance «*Glassy Metals: Magnetic, Chemical and Structural Properties»*, ed. R. Hasegawa, CRC Press, Boca Raton (1983); "*Rapidly*

Quenched Materials" eds. J. Steeb and H. Warlimont, Elsevier, Amsterdam (1985).
3. M. Hoare and P. Pal, J. Cryst. Growth, **17**, 77 (1972); C. Briant and J.J. Burton, Phys. Stat. Solidi, B **85**, 393 (1978).
4. J.-C.S. Levy, Surf. Sci. **104**, 1 (1981).
5. J.-C.S. Levy and D. Mercier, J. Appl. Phys. **53**, 7709 (1982) ; D. Mercier and J.-C.S. Levy, Phys. Rev. B **27**, 1292 (1983); D. Mercier, J.-C.S. Levy, M. Nahas, H. Huitric and M. Saintourens, J. Microsc. Spectrosc. Electr. **12**, 1 (1988).
6. D. Shechtman, I.A. Blech, D. Gratias and J.W. Cahn, Phys. Rev. Lett. **53**, 1951 (1984).
7. D. Levine and P.J. Steinhardt, Phys. Rev. Lett. **53**, 2477 (1984).
8. A.I. Gubanov, "*Quantum Theory of Amorphous Conductors"* New York, Consultant Bureau (1965); L.M. Schwartz and H. Ehrenreich, Phys. Rev. B **6**, 2923 (1972).
9. P.G. de Gennes and J. Prost, "*The Physics of Liquid Crystals*" Clarendon Press Oxford (1995); S. Chandrasekhar, "*Liquid Crystals*" Cambridge University Press (1977); P.M. Chaikin and T. Lubensky, "*Principles of Condensed Matter Physics"* Cambridge University Press (2000).
10. B.I. Halperin and D.R. Nelson, Phys. Rev. Lett. **41**, 121 (1978).
11. P.J. Lu, K. Deffeyes, P.J. Steinhardt, and N. Yao, Phys. Rev. Lett. **87**: 275507 (2001).
12. W.S. Edwards and S. Fauve, Phys. Rev. E **47**, R788 (1993); J.P. Gollub and J.S. Langer, Rev. Mod. Phys. **71**, S396 (1999).
13. H. K. Clark and J. L. Hoard, J. Am. Chem. Soc **65**, 2115 (1943); M. Hebbache, in this book.
14. M. Widom and M. Mihalkovic. Phys. Rev. B (2008), to appear.
15. R. Penrose, Eureka, **39**, 16 (1978).
16. R.M. Robinson, Inventiones Math. 12, 177 (1971).
17. R. Ammann, B. Grünbaum, and G. C. Shephard, Discrete Comput. Geom. **8**, 1 (1992) ; F. P. M. Beenker (unpublished).
18. D. Mercier, M. Perreau, J.-C.S. Levy, M. Nahas, H. Huitric, M. Saintourens, D. Berger, J.-P. Coste and S. Courmant, in « *Nouvelles Structures de Matériau*x » ed. J.-C.S. Levy, Masson, Paris, 59 (1993).
19. J. Frenkel and T. Kontorova, Phys. Z. Sowjetunion **13**, 1 (1938); F.C. Frank and J.H. van der Merwe, Proc. R. Soc. London A **198**, 205 (1949); P.M. de Wolff, Acta Cryst. A 30, 777 (1974).
20. R. Lefort, B. Toudic, J. Etrillard, F. Guillaume, P. Bourges, R. Currat and T. Breczewski, Eur. Phys. J. B **24**, 51 (2001).
21. See "*Directions in Mathematical Quasicrystals"* eds:R.V. Moody and M. Baake, CRM Monograph Series, AMS, Providence, RI (2000).
22. C. Das and H.R. Krishnamurthy, Phys. Rev. B **58**, R5889 (1998).
23. R. Berger, Memoirs of the American Mathematical Society **66**, 1 (1966).
24. P.J. Lu and P.J. Steinhardt " Science **315**, 1106 (2007).
25. D. Barache, B. Champagne and J.-P. Gazeau, Fields Inst. Monographs **10**, 15 (1998).

26. F. Scheffler, P. Maass, J. Roth and H. Stark, Eur. Phys. J. B **42**, 85 (2004).
27. F. Gähler and M. Reichert, J. Alloys and Compounds, **342**, 180 (2002).
28. J.L. Martins, J. Buttet and R. Car, Phys. Rev. B **31**, 1804 (1985). R.Kawai and J.H. Weare, J. Chem. Phys. **95**, 1151 (1991).
29. I. Boustani, A. Quandt and P. Kramer, Europhys. Lett. **36,** 583 (1996).
30. Z. Masáková, J. Patera and E. Pelantova, J. Phys. A. **31,** 1443 (1998).
31. D. Levine and P.J. Steinhardt, Phys. Rev. B **34**, 596 (1986).
32. See for instance "*Physics of Color Centers*" ed. W.B. Fowler, Academic Press, New York (1968).
33. K. Ingersent and P.J. Steinhardt, Phys. Rev. Lett. **64**, 2034 (1990).
34. N.D. Mermin, Rev. Mod. Phys. **64**, 3 (1992).
35. M. Texier, A. Joulain, J. Bonneville, L. Thilly, J. Rabier, Philos. Mag. **87**, 1497 (2007).
36. A. Bilusic, D. Pavuna and A. Smontara, Vacuum, **61**, 345 (2001).
37. E.Y. Vedmedenko, U. Grimm and R. Wiesedanger, Phys. Rev. Lett. **93**, 076407 (2003); E.Y. Vedmedenko, *"Competing Interactions and Patterns"* J. Wiley eds. Mannheim (2007).
38. G. Ceder, M. De Graef, L. Delaey, J. Kulik and D. De Fontaine, Phys. Rev. B **39**, 381 (1989).
39. L. Schwartz, *« Théorie des Distributions »* Hermann, Paris, (1967).
40. P.M. Chaikin,T.C. Lubensky, "*Principles of Condensed Matter Physics"* Cambridge University Press (2000).
41. I.N. Sneddon, "*Fourier Transforms"*, McGraw-Hill, New York (1951).
42. S. Tan, A. Ghazali and J.-C.S. Levy, Surf. Sci. **377-379**, 15 (1997); **392**, 163 (1997).
43. R. Thom, « *Stabilité Structurelle et Morphogenèse »* Interéditions, Paris, (1972).
44. H.S.M. Coxeter, «*Introduction to Geometry »* J. Wiley & sons New York (1980).
45. C. Pisot, Annali di Pisa **7**, 205 (1938) ; E. Bombieri and J.E. Taylor, J. Phys. (Paris) C**3**, 19 (1986).
46. J.-C.S. Levy and D. Mercier, Acta Physicae Superficierum **VIII**, 115 (2006).
47. P. Guyot, M. Audier, R. Lequette, J. Phys. (Paris) C**3**, 389 (1986); K. Urban, C. Mayer, M. Rapp, M. Wilkens, A. Csanady, J. Fidler, J. Phys. (Paris) C**3**, 465 (1986).
48. Y. Yan, S. Pennycook and A.P. Tsai, Phys. Rev. Lett. **81**, 5145 (1998); Y. Yan, and S. Pennycook, Phys. Rev. B **61**, 14291 (2000); Y. Yan, and S. Pennycook, Phys. Rev. Lett. **81**, 1542 (2001).
49. L. de Seze and S. Aubry, J. Phys. C **17**, 389 (1984).
50. R. Blinc, D.C. Ailion, J. Dolinsek and S. Zumer, Phys. Rev. Lett. **54**, 79 (1985).
51. M. Perreau, D. Mercier, J.-C.S. Levy and J.P. Coste, in « *Basic Features of the Glassy State*" ed. J. Colmenero and A. Alegria, World Scientific, Singapore, 73 (1990) ; M. Perreau, D. Mercier, J.-C.S. Levy and J.P. Coste in "*Nouvelles Structures de Matériaux*", ed. J.-C.S. Levy, Masson, Paris (1993) .
52. J.-C.S. Levy and D. Mercier, Eur. Phys. J. B **38**, 403 (2004).
53. N. Wang, H. Chen and K.H. Kuo, Phys. Rev. Lett. **59**, 1010 (1987).
54. N. Wang, K.K. Fung and K.H. Kuo, Appl. Phys. Lett. **52**, 2120 (1988).

55. W. Cao, H.Q. Ye and K.H. Kuo, phys. stat. sol. (a) **107**, 511 (1988).
56. J.C. Jiang, N. Wang, K.K. Fung and K.H. Kuo, Phys. Rev. Lett. **67**, 1302 (1991); C. Jiang, K.K. Fung and K.H. Kuo, Phys. Rev. Lett. **68**, 616 (1992).
57. Y. Lai, X. Zhang and Z.-Q. Zhang, J. Appl. Phys. **91**, 6191(2002).
58. J. Saida, M. Matsushita and A. Inoue, J. Appl. Phys. **88**, 6081(2002).